Synergetic Fluid Mixing from Viscous Fingering and Alternating Injection

Birendra Jha, Luis Cueto-Felgueroso, and Ruben Juanes*

Massachusetts Institute of Technology, 77 Massachusetts Avenue, Building 48, Cambridge Massachusetts 02139, USA
(Received 4 April 2013; published 1 October 2013)

We study mixing of two fluids of different viscosity in a microfluidic channel or porous medium. We show that the synergetic action of alternating injection and viscous fingering leads to a dramatic increase in mixing efficiency at high Péclet numbers. Based on observations from high-resolution simulations, we develop a theoretical model of mixing efficiency that combines a hyperbolic mixing model of the channelized region ahead and a mixing-dissipation model of the pseudosteady region behind. Our macroscopic model quantitatively reproduces the evolution of the average degree of mixing along the flow direction and can be used as a design tool to optimize mixing from viscous fingering in a microfluidic channel.

PACS numbers: 47.51.+a, 47.15.gp, 47.20.Gv, 47.56.+r

Efficient fluid mixing at low Reynolds numbers is challenging because one cannot rely on either turbulence or inertial effects to induce disorder in the velocity field. Several strategies have been proposed to achieve fast mixing in small devices such as microfluidic cells [1,2], including grooved walls [3], bubble capillary flows [4], pulsating injection [5], electroosmosis [6], electrokinetics [7], and acoustic stimulation [8]. Alternating injection of two fluids has also been proposed to enhance mixing in laminar-flow conditions [9,10].

Recently, we have shown that miscible viscous fingering—a hydrodynamic instability that takes place when a less viscous fluid displaces a more viscous fluid—can enhance mixing in periodic Darcy flows, such as flows in Hele-Shaw cells or porous media [11]. Enhanced mixing due to viscous fingering emerges from the velocity disorder and the additional interfacial area created between the two fluids as a result of the hydrodynamic instability. Creation of new fluid-fluid interfaces is accelerated by tip splitting of the fingers and retarded by channeling, which are the two primary mechanisms controlling the dynamics of viscous fingering [11–14]. Fluid mixing from viscous fingering is determined by the delicate balance of these two mechanisms.

Periodic flows, however, while conceptually important to gain understanding, are difficult to achieve in practice. Here, we study mixing of two miscible fluids of different viscosities due to the combined effect of viscous fingering and alternating injection and find that the two can act synergistically to achieve rapid mixing at low Reynolds numbers and high Péclet numbers, typical of microfluidic flows. We perform high-resolution numerical simulations that elucidate the phenomenon and guide us to formulate a macroscopic model that captures the universal signature of mixing from viscous fingering and alternating injection. Previous studies of viscous fingering in alternating injection [e.g.,[14–16]] analyze *spreading* of a single slug as a result of viscous fingering, where the quantities of interest are the transverse-averaged concentration and the

longitudinal variance of the concentration field. However, it is *mixing*, not spreading, that controls chemical reactions and dilution of peak concentrations [17], a process that requires estimating the variance of the concentration field [18,19].

We consider flow of two fluids of different viscosities μ_1 and μ_2, where $\mu_1 < \mu_2$, through a homogeneous two-dimensional porous medium or a Hele-Shaw cell (two parallel plates separated by a thin gap). We adopt a Darcy formulation, which is well accepted for single-phase flows in porous media [20] and has been used extensively to model flow in a Hele-Shaw cell for a range of Péclet numbers and viscosity ratios [12,13,21–24]. Although three-dimensional effects could play a role in a viscously unstable Hele-Shaw flow, these would require 3D Stokes simulations that would incur in a formidable computational cost, and likely would not introduce a fundamental qualitative departure from our findings. The porosity ϕ and permeability k are constant. The length and width of the domain are L and W, respectively. We define concentration c as the volume fraction of the less viscous fluid in the mixture. We assume that the more viscous fluid completely fills the cell initially. We assume an exponential viscosity model $\mu(c) = \mu_1 e^{R(1-c)}$, where $R = \ln M$ and $M = \mu_2/\mu_1$ is the viscosity contrast. We simulate alternating injection, in which one cycle corresponds to a slug of the less viscous fluid entering the flow cell at constant rate from the left boundary followed by a slug of the more viscous fluid at the same rate. Let $A_s = \phi W l_s$ be the volume of the less viscous slug. The mean velocity is in the x direction and of magnitude U. The outlet is a natural outflow boundary. The two fluids are assumed to be first-contact miscible, neutrally buoyant, and incompressible. First-contact miscibility means the fluids mix instantaneously in all proportions to form a single phase and surface tension effects are absent. Like in many previous studies on viscous fingering [16,23–25], the diffusion coefficient D between the fluids is assumed to be constant, isotropic, and independent of concentration. Although D is likely velocity dependent,

this effect appears not to play a major role on macroscopic features of viscous fingering at high Péclet numbers and late times [13], and a hydrodynamic dispersion model for flows with large viscosity contrast, especially in the pre-asymptotic regime, is still lacking [23,26]. To nondimensionalize the system, we choose the "slug length" l_s as the characteristic length, U as the characteristic velocity, μ_1 as the characteristic viscosity, $P = \mu_1 U l_s / k$ as the characteristic pressure, and $T = \phi l_s / U$ as the characteristic time. The governing equations in dimensionless form are [22]

$$\partial_t c + \nabla \cdot \left(\boldsymbol{u} c - \frac{1}{\mathrm{Pe}} \nabla c \right) = 0, \qquad (1)$$

$$\boldsymbol{u} = -\frac{1}{\mu(c)} \nabla p, \qquad \nabla \cdot \boldsymbol{u} = 0, \qquad (2)$$

in $x \in [0, L/l_s]$ and $y \in [0, W/l_s]$, where $\boldsymbol{u} = [u, v]$ and p are the velocity and pressure fields. The initial condition is $c|_{t=0} = 0$. The boundary conditions are $c|_{y=0} = c|_{y=W/l_s}$ (periodic in y), $\boldsymbol{u} \cdot \boldsymbol{n}|_{x=0} = -1$ (inflow), $p|_{x=L/l_s} = 0$ (outflow), and alternating injection

$$(\boldsymbol{u} \cdot \boldsymbol{n}) c|_{x=0} = \begin{cases} -1 & \text{if } 0 < \mathrm{rem}(t, 1/r_s) \leq 1 \\ 0 & \text{if } 1 < \mathrm{rem}(t, 1/r_s) < 1/r_s, \end{cases} \qquad (3)$$

where $\boldsymbol{n}$ is the outward unit normal and $\mathrm{rem}(\cdot)$ is the remainder function. We fix the aspect ratio $L/W = 8$ and the slug ratio $r_s = 0.5$ (1:1 fluid volume ratio). The slug ratio is also the dimensionless concentration of the perfectly mixed fluid. The dimensionless parameters governing fluid mixing are the Péclet number $\mathrm{Pe} = U l_s / D$, the log-viscosity contrast R in the viscosity law, and the dimensionless length L/l_s of the channel.

We discretize Eq. (1) using sixth-order compact finite differences in the streamwise direction and the fast Fourier transform in the transverse direction, which is periodic [23,25,27]. We advance in time using a third-order Runge-Kutta scheme. To gain numerical stability at high M, we solve the pressure equation (2) directly using finite volumes with a two-point flux approximation, instead of using the stream function vorticity approach [22]. Figure 1 shows a snapshot of the concentration field from an alternating-injection simulation.

Fluid mixing results in decay of the concentration variance, and the mean scalar dissipation rate determines the rate of this decay [11,18,28,29]. To investigate mixing in a channel under alternating injection, we study the transversely averaged profiles of the degree of mixing and the scalar dissipation rate. While these profiles oscillate with time as the slugs of the two pure fluids enter the domain in alternating fashion, time averaging leads to slowly varying longitudinal profiles. We define the longitudinal concentration variance $\overline{\sigma^2}(x, t) \equiv \overline{c^2} - \bar{c}^2$, the longitudinal degree of mixing $\bar{\chi}(x, t) \equiv 1 - \overline{\sigma^2}/\sigma_{\max}^2$, and the longitudinal scalar dissipation rate $\bar{\epsilon}(x, t) \equiv \overline{|\boldsymbol{g}|^2}/\mathrm{Pe}$, where $\boldsymbol{g} \equiv \nabla c$
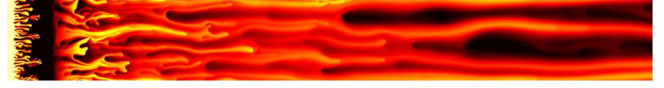

FIG. 1 (color online).   Snapshot of the concentration field during the alternating injection of more-viscous (dark) and less-viscous (light) fluids. Viscous fingering at the displacement front promotes mixing of the two fluids. At high viscosity contrast, however, a few dominating fingers coalesce to form persistent channels. These channels serve as preferential pathways for subsequent slugs of the less-viscous fluid, inhibit transverse mixing, and shield growth of adjacent fingers. The displacement corresponds to a viscosity ratio $M \approx 33$ ($R = 3.5$) and Péclet number $\mathrm{Pe} = 2000$. See Supplemental Material for videos [39].

and $\overline{(\cdot)} \equiv \int_0^{W/l_s} \int_{t-t_w/2}^{t+t_w/2} (\cdot) dt' dy$ denotes averaging in the transverse direction and in time (we average over a time window t_w of three injection cycles).

The fundamental observation is the development of three distinct mixing regions along x (Fig. 2). Region I, closest to the inlet, is a region of active mixing as a result of the vigorous interaction between fingers from intermittent injection of the less-viscous fluid. Region II is a well-mixed region, whose extent grows over time. Region III is a region of poorly mixed fluid ahead of the well-mixed region, dominated by the presence of channels of well-mixed fluid that penetrate through the ambient, more viscous fluid. We have confirmed with simulations (not shown here) that the behavior of the system is qualitatively and quantitatively the same even if the effect of Korteweg stresses [30] is included in the formulation.

The key descriptor of the flow is the location of the well-mixed front $x_f(t)$ separating regions II and III, as a function of time. This front corresponds to the position at which the average degree of mixing is maximum, $\bar{\chi}_f(t) = \max_x \bar{\chi}(x, t)$ [Fig. 2(e)]. It also corresponds to the point at which the transverse average of the scalar dissipation rate is minimum, $\bar{\epsilon}_f(t) = \min_x \bar{\epsilon}(x, t)$ [Fig. 2(f)].

We now formalize these qualitative observations and develop an analytical model of the average degree of mixing in the channel. We formulate two submodels: one for the channelized region (III), and one for the active-mixing and well-mixed regions (I and II). Each submodel originates from the exact average equations of mean concentration $\bar{c}$, concentration variance $\overline{\sigma^2}$, and mean scalar dissipation rate $\bar{\epsilon}$. For example, we obtain the exact equations for $\bar{c}$ and $\overline{c^2}$ by premultiplying the advection-diffusion equation (1) by 1 and c, respectively, integrating in y, making use of the divergence theorem, and incorporating periodicity in y:

$$\partial_t \bar{c} + \partial_x \left(\overline{uc} - \frac{1}{\mathrm{Pe}} \partial_x \bar{c} \right) = 0, \qquad (4)$$

$$\partial_t \overline{c^2} + \partial_x \left(\overline{uc^2} - \frac{1}{\mathrm{Pe}} \partial_x \overline{c^2} \right) = -2\bar{\epsilon}. \qquad (5)$$
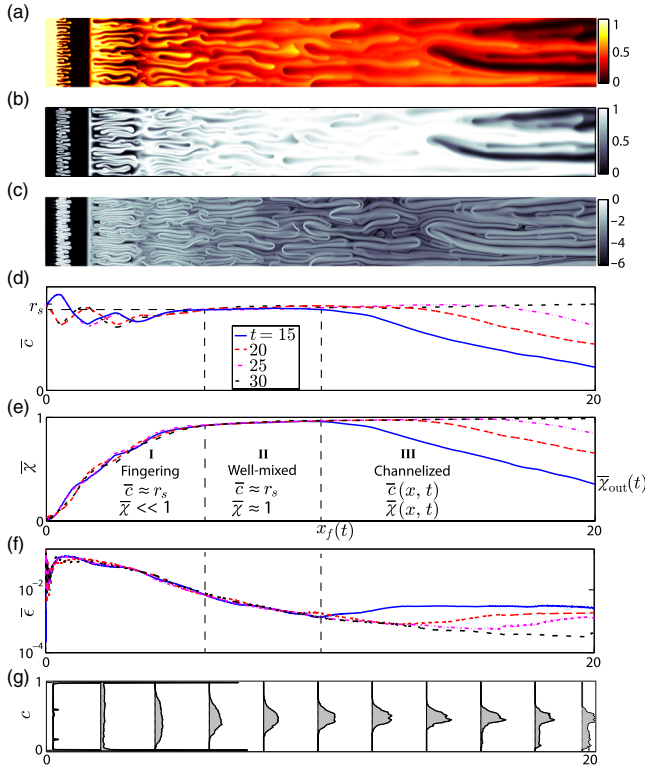
FIG. 2 (color online). (a) Concentration c, (b) degree of mixing χ, and (c) scalar dissipation rate $\log\epsilon$ from an alternating injection simulation with viscosity ratio $M = \exp(2) \approx 7$ and Péclet number Pe = 2000 at time $t = 18.6$. the degree of mixing is high (white) where mixing has already taken place. Scalar dissipation rate is high (white) at the interfaces where the fluid is actively being mixed. (d)–(f) Longitudinal profiles of concentration $\bar{c}$, degree of mixing $\bar{\chi}$, and scalar dissipation rate $\bar{\epsilon}$, averaged over a moving time window (of duration equal to 3 injection cycles, although the same behavior holds for different averaging windows). $\bar{\epsilon}$ reaches a maximum where fingering begins and a minimum where channeling begins, congruent with a nonmonotonic degree of mixing $\bar{\chi}$ with x. (g) The time-averaged probability density function (PDF) of concentration evolves from two deltalike functions (segregated pure fluids near $x = 0$ in region I) to a Gaussian-like function (well-mixed fluids in region II) to an anomalous distribution (channeling in region III). The vertical dashed lines indicate the boundaries of the three mixing regions at time $t = 15$; x_f denotes the position of the well-mixed front, which is the position of the maximum longitudinal degree of mixing in the domain $\bar{\chi}_f$ at a given time.

Region III is characterized by channeling, where the less-viscous fluid spreads longitudinally through fast-moving channels ahead of the well-mixed front. This dominance of heterogeneous fluid displacement over mixing suggests that we can pose a hyperbolic model by neglecting diffusion. The development of hyperbolic models (also called fractional flow formulations) of *average* concentrations that capture the fingering-enhanced *spreading* has a long history [31–33]. Here, we extend this approach to develop a hyperbolic fractional-flow model

of *mixing*, which of course must involve higher-order moments of the concentration field. Neglecting diffusion in Eqs. (4) and (5) (that is, taking Pe $\to \infty$), we obtain a hyperbolic approximation for the propagation of the mean concentration and the mean scalar energy: $\partial_t \bar{c} + \partial_x \overline{uc} = 0$ and $\partial_t \overline{c^2} + \partial_x \overline{uc^2} = 0$, respectively. Combining these equations we immediately obtain a hyperbolic approximation for the average degree of mixing $\bar{\chi}$:

$$\partial_t \bar{\chi} + \partial_x \overline{u\chi} = 0. \tag{6}$$

We provide closure for this equation with a fractional-flow formulation, in which we model $\overline{u\chi}$ as a function of $\bar{\chi}$ alone: the fractional-flow function $f(\bar{\chi})$. Different models of the fractional-flow function have been proposed for the *mean* concentration [e.g.,[33–35]]. Here we use

$$f(\bar{\chi}) = \frac{M_{\text{eff}}\bar{\chi}}{1 + (M_{\text{eff}} - 1)\bar{\chi}},$$
$$M_{\text{eff}} = (\alpha + (1 - \alpha)M^{(1-r_s)/4})^4, \tag{7}$$

where α is the mixing ratio, defined as the degree of mixing in the "effective" displacing fluid in the channelized region III, and M_{eff} is the *effective* viscosity ratio of the more-viscous to the less-viscous fluid in the channelized region, estimated using the quarter-power mixing rule. Equation (7) is based on Koval's model [33], modified for region III where the less-viscous fluid in the channels—with average concentration $c = r_s$—displaces the more-viscous fluid with $c = 0$. The function (7) is concave, so the solution to Eq. (6) is a rarefaction wave where the derivative $\zeta = f'(\bar{\chi})$ is the speed of propagation of degree of mixing $\bar{\chi}$ [36]. The solution at different times can therefore be understood as a simple stretching of the characteristic velocity ζ.

We test the validity of this fractional-flow model by comparing the model predictions with direct numerical simulations (Fig. 3). In the channeling region, the averaged degree of mixing from simulations indeed behaves as a continuous rarefaction wave that stretches with time, and this is captured nicely by the analytical model. From the
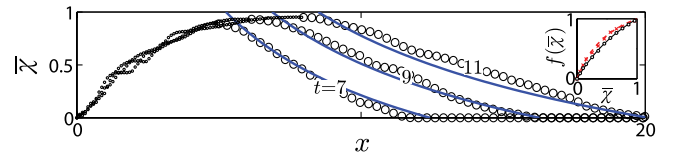

FIG. 3 (color online). Time evolution of the profiles of average degree of mixing $\bar{\chi}$, for $R = 2$ and Pe = 2000. The results from averaging a high-resolution simulation in the channelized region (large circles) are well captured by the hyperbolic mixing model (blue solid lines). Shown are three different times ($t = 7$, 9, and 11) that illustrate the self-similar $x \sim t$ character of the degree of mixing in the channelized region. Inset: Fractional-flow function obtained from averaging of the direct numerical simulations (symbols) and from the proposed model (7) with $\alpha = 0.5$, for $R = 2$ (black circles) and $R = 3.5$ (red crosses).
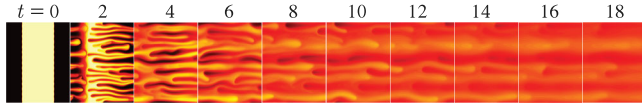
FIG. 4 (color online).   Snapshots from a periodic-flow simulation at successive times for $R = 2$ and Pe = 2000. Note the similarity with an alternating injection simulation (Fig. 2), especially away from the inlet and outlet boundaries. The domain length in the periodic simulation corresponds to one injection cycle: in this case, one-tenth of the domain length in the alternating injection simulation.

profiles of average degree of mixing at different times in the channelized region we compute the numerical fractional-flow function, which is well approximated for a wide range of viscosity contrasts M by function (7) with a single value of the mixing ratio, $\alpha = 0.5$ (Fig. 3, inset).

We now turn our attention to modeling regions I and II. Because these are regions of active mixing, one cannot neglect diffusion. We develop a mixing model from the exact equations of average concentration variance $\overline{\sigma^2}$ and average scalar dissipation rate $\bar{\epsilon}$. We obtain the former by combining Eqs. (4) and (5) and the latter by taking the gradient of the advection-diffusion equation (1) and then the dot product with ∇c, integrating in y and exploiting periodicity in y:

$$\partial_t \bar{\epsilon} + \partial_x \left(\overline{u\epsilon} - \frac{1}{\text{Pe}} \partial_x \bar{\epsilon} \right) = -\frac{2}{\text{Pe}} \overline{\nabla u : g \otimes g} - \frac{2}{\text{Pe}^2} \overline{\nabla g : \nabla g}.$$

(8)

From Figs. 2 and 3, it is clear that in regions I and II the average degree of mixing $\bar{\chi}$ reaches a steady-state profile, and therefore can be described as a function of x only. The fundamental observation is that the flow approaches statistical homogeneity due to the many tip-splitting and finger-merging events and that the diffusive component of the generalized flux is much smaller than the advective component, $\partial_{xx}\overline{(\cdot)}/\text{Pe} \ll \partial_x \overline{u(\cdot)}$. As a result, the spatial
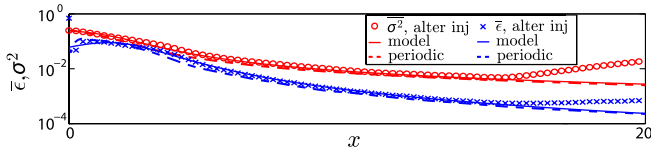

FIG. 5 (color online).   Average concentration variance ($\overline{\sigma^2}$, red) and scalar dissipation rate ($\bar{\epsilon}$, blue) from the alternating injection simulations (symbols), the analytical dissipation model (thin solid lines), and periodic simulations (dashed lines) for $R = 2$, Pe = 2000, at time $t = 22$. The results from the periodic simulation are computed by averaging over the entire volume at every time step, and the x axis for these curves is time t. The values of the constants in the dissipation model [11] are $A = 0.89$, $B = 0.51$. The model departs from the simulations ahead of the well-mixed front x_f, where the hyperbolic model applies instead (region III, Fig. 3).

variation in average quantities ($\bar{c}$, $\overline{c^2}$, $\bar{\epsilon}$) can be understood as the temporal variation of a parcel of fluid moving with mean velocity $\bar{u}$ ($= 1$ in the nondimensional equations). In other words, we can approximate $\partial_t(\cdot) + \partial_x \overline{u(\cdot)} \approx d\overline{(\cdot)}/dt$. This is illustrated in Fig. 4, which shows that a concatenation of snapshots from a simulation in a periodic domain of length equal to one injection cycle, under the space-time mapping $x = t$, closely resembles the concentration field in regions I and II in the full simulation of alternating injection [Fig. 2(a)].

From our key observation of space-time duality, the final approximate equations that require modeling are the average variance and scalar dissipation rate in a biperiodic domain. A macroscopic model of mixing due to viscous fingering under periodic boundary conditions was recently developed [11,27]. We have confirmed that the predictions from this analytical model are in excellent agreement with direct numerical simulations of alternating injection (Fig. 5), and we refer to [11,27] for the details of this mixing-dissipation model.

We now put the two submodels together: the dissipation model in regions I and II and the hyperbolic model in region III. We use the analytical model to explore the influence of the system parameters on mixing efficiency by considering two practical measures: the minimum time to achieve a desired degree of mixing [Fig. 6(a)] and the maximum degree of mixing at the outlet (that is, the degree of mixing of the effluent mixture at long times) [Fig. 6(b)]. We find that a viscosity contrast between the fluids leads to
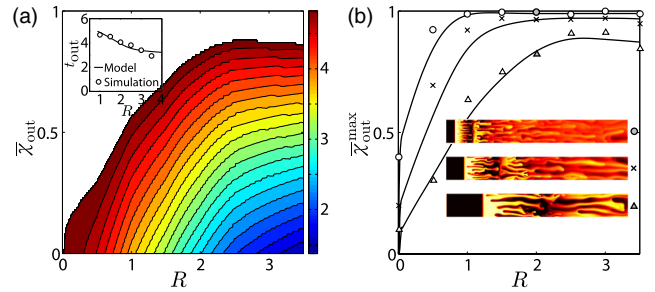

FIG. 6 (color online).   (a) Contours of the mixing time t_{out} as a function of the *desired* degree of mixing at the outlet $\bar{\chi}_{\text{out}}$ and the log-viscosity contrast R, for a domain of dimensionless length $L/l_s = 5$ and Pe = 4800. The white region beyond the outermost contour indicates values of $\bar{\chi}_{\text{out}}$ that cannot be achieved for those flow conditions. The inset shows the comparison of mixing time for $\bar{\chi}_{\text{out}} = 0.5$ between the mixing model and the simulations. (b) Maximum attainable degree of mixing at the outlet $\bar{\chi}_{\text{out}}^{\max}$ as a function of R for different slug sizes l_s. As l_s decreases, the Péclet number Pe = Ul_s/D decreases and the dimensionless domain length L/l_s increases, which results in a higher degree of mixing. Shown are three cases: $L/l_s = 5$ (triangles), 10 (crosses), 20 (circles); Pe = 4800, 2400, 1200 in the same order. Solid line is from the mixing model, and symbols are from the numerical simulations. The insets show snapshots of the concentration field at long times for $R = 2$ and different slug sizes: $L/l_s = 5$ (bottom), 10 (middle), 20 (top).

a dramatic increase in mixing efficiency. Mixing from alternating injection of equal-viscosity fluids ($R = 0$) is extraordinarily inefficient at all practical Péclet numbers [Fig. 6(a)]. Our analysis provides a natural explanation for the effect of slug size. Decreasing slug size l_s (that is, increasing alternating-injection frequency) leads to both a decrease in Péclet number Pe $= U l_s / D$ and an increase in dimensionless channel length L/l_s, and therefore results in a higher degree of mixing [Fig. 6(b)]. Mixing efficiency, however, does not necessarily increase uniformly with viscosity contrast between the fluids. For a given Péclet number and dimensionless channel length, there is a viscosity contrast for which the attainable degree of mixing of the effluent mixture is maximized. This optimum viscosity contrast promotes rapid creation of interfacial area from viscous fingering while disallowing strong channeling effects.

In conclusion, we have shown that the synergetic action of alternating injection and viscous fingering leads to a dramatic increase in efficiency when mixing fluids at high Péclet numbers—a notoriously challenging problem in the context of planar microfluidic devices as lab-on-a-chip systems [37,38].

---

*juanes@mit.edu

[1] H. A. Stone, A. D. Strook, and A. Ajdari, Annu. Rev. Fluid Mech. **36**, 381 (2004).
[2] J. M. Ottino and S. Wiggins, Phil. Trans. R. Soc. A **362**, 923 (2004).
[3] A. D. Strook, S. K. W. Dertinger, A. Ajdari, I. Mezic, H. A. Stone, and G. M. Whitesides, Science **295**, 647 (2002).
[4] P. Garstecki, M. J. Fuerstman, M. A. Fischbach, S. K. Sia, and G. M. Whitesides, Lab Chip **6**, 207 (2006).
[5] I. Glasgow and N. Aubry, Lab Chip **3**, 114 (2003).
[6] I. Glasgow and N. Aubry, Lab Chip **4**, 558 (2004).
[7] J. D. Posner, C. L. Perez, and J. G. Santiago, Proc. Natl. Acad. Sci. U.S.A. **109**, 14 353 (2012).
[8] T. Frommelt, M. Kostur, M. Wenzel-Schäfer, P. Talkner, P. Hänggi, and A. Wixforth, Phys. Rev. Lett. **100**, 034502 (2008).
[9] J. M. MacInnes, Z. Chen, and R. W. K. Allen, Chem. Eng. Sci. **60**, 3453 (2005).
[10] J. T. Coleman and D. Sinton, Microfluid. Nanofluid. **1**, 319 (2005).
[11] B. Jha, L. Cueto-Felgueroso, and R. Juanes, Phys. Rev. Lett. **106**, 194502 (2011).
[12] G. M. Homsy, Annu. Rev. Fluid Mech. **19**, 271 (1987).
[13] W. B. Zimmerman and G. M. Homsy, Phys. Fluids A **3**, 1859 (1991).
[14] M. Mishra, M. Martin, and A. De Wit, Phys. Rev. E **78**, 066306 (2008).
[15] C.-Y. Chen and S.-W. Wang, International Journal of Numerical Methods for Heat and Fluid Flow **11**, 761 (2001).
[16] A. De Wit, Y. Bertho, and M. Martin, Phys. Fluids **17**, 054114 (2005).
[17] M. Dentz, T. Le Borgne, A. Englert, and B. Bijeljic, J. Contam. Hydrol. **120–121**, 1 (2011).
[18] T. Le Borgne, M. Dentz, D. Bolster, J. Carrera, J.-R. de Dreuzy, and P. Davy, Adv. Water Resour. **33**, 1468 (2010).
[19] D. Bolster, F. J. Valdes-Parada, T. Le Borgne, M. Dentz, and J. Carrera, J. Contam. Hydrol. **120–121**, 198 (2011).
[20] J. Bear, *Dynamics of Fluids in Porous Media* (Wiley, New York, 1972).
[21] D. Bensimon, L. P. Kadanoff, S. Liang, B. I. Shraiman, and C. Tang, Rev. Mod. Phys. **58**, 977 (1986).
[22] C. T. Tan and G. M. Homsy, Phys. Fluids **31**, 1330 (1988).
[23] M. Ruith and E. Meiburg, J. Fluid Mech. **420**, 225 (2000).
[24] A. De Wit, Phys. Rev. Lett. **87**, 054502 (2001).
[25] C. Y. Chen and E. Meiburg, J. Fluid Mech. **371**, 233 (1998).
[26] P. Petitjeans, C.-Y. Chen, E. Meiburg, and T. Maxworthy, Phys. Fluids **11**, 1705 (1999).
[27] B. Jha, L. Cueto-Felgueroso, and R. Juanes, Phys. Rev. E **84**, 066312 (2011).
[28] S. B. Pope, *Turbulent Flows* (Cambridge University Press, Cambridge, England, 2000).
[29] J. J. Hidalgo, J. Fe, L. Cueto-Felgueroso, and R. Juanes, Phys. Rev. Lett. **109**, 264503 (2012).
[30] C.-Y. Chen, L. Wang, and E. Meiburg, Phys. Fluids **13**, 2447 (2001).
[31] R. J. Blackwell, J. R. Rayne, and W. M. Terry, Pet. Trans. AIME **217**, 1 (1959).
[32] B. Habermann, Pet. Trans. AIME **219**, 264 (1960).
[33] E. J. Koval, Soc. Pet. Eng. J. **3**, 145 (1963).
[34] M. R. Todd and W. J. Longstaff, J. Pet. Technol. **24**, 874 (1972).
[35] F. J. Fayers, Soc. Pet. Eng. Res. Eng. **3**, 551 (1988).
[36] C. M. Dafermos, *Hyperbolic Conservation Laws in Continuum Physics* (Springer-Verlag, Berlin, 2000).
[37] M. Hashimoto, P. Garstecki, H. A. Stone, and G. M. Whitesides, Soft Matter **4**, 1403 (2008).
[38] T. Ahmed, T. S. Shimizu, and R. Stocker, Integr. Biol. **2**, 604 (2010).
[39] See Supplemental Material at http://link.aps.org/supplemental/10.1103/PhysRevLett.111.144501 for simulation videos.